Consistent Nonlinear Elastic Image Registration

G. E. Christensen and J. He
Department of Electrical and Computer Engineering
The University of Iowa
Iowa City, IA, 52242

Abstract

This paper describes a new bidirectional image registration algorithm that estimates a consistent set of nonlinear forward and reverse transformations between two N-dimensional images. The registration problem is formulated in a N+1-dimensional space where the additional dimension is referred to as the temporal or time dimension. A periodic-in-time, nonlinear, N+1-dimensional transformation is estimated that deforms one image into the shape of the other and back again. The registration problem is solved numerically by discretizing the temporal dimension such that there is an incremental image and transformation at each time point. Nonlinear deformations from one image to the other are accommodated by concatenating the linear, small-deformation incremental transformations. An inverse consistency constraint is placed on the incremental transformations to enforce within a specified tolerance that the forward and reverse transformations between the two images are inverses of each other. Results are presented for 2D image registration problems. These results demonstrate the feasibility of accommodating both linear and nonlinear deformations.

1. Introduction

The goal in image registration is to find a transformation that defines the pointwise correspondence between objects contained within the images being registered. The correspondence between objects that differ slightly in shape such as the small and large squares in Fig. 1 can be described using a small-deformation, linear transformation model. However, objects that have large shape differences such as the circle and "C" shown in Fig. 1 require a large-deformation, nonlinear transformation model. In this paper we present a new bidirectional image registration algorithm that estimates a consistent set of nonlinear forward and reverse transformations between two images. This method accommodates large nonlinear deformations by concatenat-

ing a sequence of small incremental transformations from the domain of one image to that of the other. Inverse consistency between the forward and reverse transformations is achieved by jointly estimating the incremental transformations while enforcing inverse consistency constraints on each incremental transformation. The transformation estimation is regularized using a linear differential operator that penalizes second order derivatives in both the spatial and temporal dimensions. This regularization is most similar to a thin-plate spline or linear elastic regularization with the difference that it is applied to both the spatial and temporal dimensions instead of just the spatial dimension.

Figure 1. Simple objects used to test the image registration algorithm.

Registration methods that accommodate large-deformation, nonlinear transformations are often based on continuum mechanical models such as hyperelasticity[10] and viscous fluids [3, 5, 7, 8, 1, 9]. In the case of a hyperelasticity model, one image is deformed into the shape of the other assuming that it is a fully elastic material while accommodating the nonlinear behavior due to the path of the deformation. Registration algorithms based on the viscous fluid transformation model accommodate locally large nonlinear deformations by modeling the deformation of one image into the shape of the other as a fluid material. The method presented in this paper is most similar to the hyperelastic material model since the regularization is applied to the displacement field as opposed to the velocity field which would be the case for a viscous fluid material.

The idea of inverse consistent image registration was first presented for linear transformations by Woods et al. [12]. In their approach, inverse consistency was achieved for a population of data sets by iteratively minimizing the pairwise

consistency error. The first nonrigid registration algorithm to correct for inverse consistency errors was put forth by Thirion[11]. In Thirion's work, a set of inverse consistent transformations are achieved by iteratively minimizing the residual of the inverse consistency error using a first order Taylor series approximation. In our previous work, we introduced the idea of inverse consistent image registration [2, 4, 6] in which forward and reverse transformations are estimated jointly while enforcing the forward and reverse transformations to be inverse consistent. In this approach, the inverse transformations are explicitly calculated without the need for any small deformation or linearization approximations. The algorithm presented in this paper extends the previous consistent, small deformation approach to the case of nonlinear inverse consistent image registration.

2. Methods

2.1. Notation

This section describes the notation and assumptions used through out the paper to describe N+1D periodic images and transformations (see Figure 2). For convenience of presentation, we will assume that there are three spatial dimensions and one temporal dimension. Both continuous and discrete notation is used because applying a transformation to an image is an inherently continuous operation while representing images and computer processing are inherently discrete operations.

Let $\Omega_d = \{(n_1, n_2, n_3, n_4) : 0 \le n_1 < N_1, 0 \le n_2 < N_2, 0 \le n_3 < N_3, 0 \le n_4 < N_4\}$ be the index set of image domain lattice and $N = [N_1, N_2, N_3, N_4]$. Without loss of generality, N_4 will be assumed to be an even number throughout the paper.

Let T_c denote a continuous 4D image defined on the domain $\Omega_x \times \Omega_t$ where $\Omega_x = [0, 1)^3$ denotes the 3D spatial domain and $\Omega_t = [0, 1)$ denotes the 1D temporal domain. Let T_d denote the discrete version of T_c produced by sampling T_c using the standard formula $T_d[n] = T_c\left(\frac{n}{N}\right)$ for $n \in \Omega_d$ and where $\left(\frac{n}{N}\right) = \left[\frac{n_1}{N_1}, \frac{n_2}{N_2}, \frac{n_3}{N_3}, \frac{n_4}{N_4}\right]$. In this work, the continuous image T_c is constructed from the discrete image T_d using trilinear interpolation.

A continuous image T_c is said to be periodic iff $T_c(x_1 + k_1, x_2 + k_2, x_3 + k_3, x_4 + k_4) = T_c(x_1, x_2, x_3, x_4)$ for all $x \in \Omega_x \times \Omega_t$ and a discrete image T_d is said to be periodic iff $T_d[n_1 + k_1 N_1, n_2 + k_2 N_2, n_3 + k_3 N_3, n_4 + k_4 N_4] = T_d[n_1, n_2, n_3, n_4]$ for all $n \in \Omega_d$, where k_1, k_2, k_3, and k_4 are integers.

Figure 2 shows a 4D image that has been sampled eight times (i.e., $N_4 = 8$) in the temporal dimension and the transformations that transform one image into the shape of the next. A transformation is said to be diffeomorphic if it is one-to-one, onto, and differentiable. Let $\mathcal{H}$ denote the set of all periodic diffeomorphic transformations that maps the domain $\Omega_x \times \Omega_t$ to Ω_x. The transformation $h(x, i) \in \mathcal{H}$ is defined as the transformation that maps image i into image $i + 1$, that is defines the correspondence between coordinate system of image i and that of image $i + 1$. Let $u(x, i) = h(x, i) - x$ denote the displacement field associated with the forward transformation h and let $\tilde{u}(x, i) = h^{-1}(x, i) - x$ denote the displacement field associated with the inverse transformation h^{-1}.

2.2. Image Registration

This section describes how two 3D images I_0 and I_1 are registered by constructing a 4D image T that is periodic in both the spatial and temporal dimensions. The 4D image T is defined as a sequence of 3D images indexed by time that smoothly changes shape from image I_0 at time $t = 0$ to the image I_1 at time $t = 0.5$ and back again at time $t = 1$.

Let $I_0(x)$ and $I_1(x)$ for $x \in \Omega_x$ denote two 3D images to be registered. Let the image T_c denote a 4D, continuous-in-time[1], periodic extension of I_0 and I_1 on $\Omega_x \times \Omega_t$ such that $T_c(x, 0) = I_0(x)$ and $T_c(x, 0.5) = I_1(x)$. Let T and h denote the time-sampled versions of T_c and h_c, respectively, with N_4 uniformly spaced time samples on Ω_t, such that

$$
\begin{aligned}
&T(x, 0) = I_0(x), && T(x, 1) = T(h(x, 0), 0), \\
&T(x, 2) = T(h(x, 1), 1), && T(x, 3) = T(h(x, 2), 2), \\
&T(x, 4) = I_1(x), && T(x, 5) = I_1(h(x, 4)), \\
&T(x, 6) = T(h(x, 5), 5), && T(x, 7) = T(h(x, 6), 6)
\end{aligned}
$$

for the case $N_4 = 8$. The spatial transformations $h(x, \cdot)$ can be composed together to produce the intermediate time samples of T from the original images, i.e.,

$$
\begin{aligned}
&T(h(x, 3), 3) = I_0(h(h(h(h(x, 3), 2), 1), 0)) \quad \text{and} \\
&T(h(x, 7), 7) = I_1(h(h(h(h(x, 7), 6), 5), 4)). \quad (1)
\end{aligned}
$$

For notational convenience, let S denote a time shifted version of the template image T such that

$$ S(x, i) = T(x, i + 1) \qquad 0 \le i < N_4 \qquad (2) $$

Image S is assumed to be constant during each iteration of the transformation parameter estimation (see next section) and is updated after each estimation iteration.

A necessary condition to insure a biologically realistic transformation[2] between two images is that the forward and

[1]Continuous-in-time refers to T_c being continuous in the fourth argument of T_c

[2]True biological correspondence only makes sense when comparing images from the same individual. A biologically realistic correspondence is a biologically meaningful pointwise correspondence between images of different people and is task dependent.
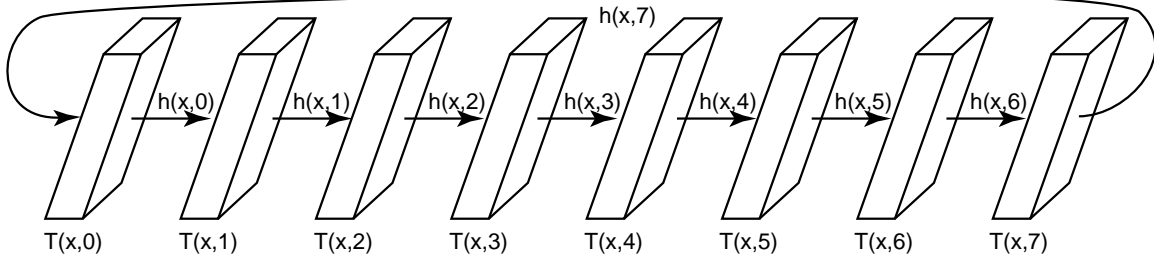
Figure 2. N+1D image and associated incremental transformations.

reverse transformations are inverses of one another. This is accomplished by placing an inverse-consistency constraint [4] on the transformation h that defines the correspondence between the temporal subimages of T. Eq. 1 implies that the forward and reverse transformations that map I_0 to I_1 and back are given by

$$h_{\text{for}}(x) = h(h(h(h(x,3),2),1),0) \quad \text{and}$$
$$h_{\text{rev}}(x) = h(h(h(h(x,7),6),5),4), \tag{3}$$

respectively. The inverse-consistency constraint implies that the composition of the forward and reverse transformations produce the identity mapping, i.e., $h_{\text{for}}(h_{\text{rev}}(x)) = h_{\text{rev}}(h_{\text{for}}(x)) = x$.

The inverse consistency constraint for the 4D transformation is imposed by enforcing the constraints

$$h(x,i) = h^{-1}(x, N_4 - 1 - i) \tag{4}$$

for $0 \leq i < N_4$. These constraints imply that each intermediate image $T(x,i)$ has the approximate appearance of the image $T(x, N_4 - i)$ for $0 \leq i < N_4$, i.e., $T(x,i) \sim T(x, N_4 - i)$ for $x \in \Omega_x$.

The 4D image registration problem is formulated as the minimization with respect to h of the cost function

$$C(h) = \sigma \sum_{i=0}^{N_4-1} \int_{\Omega_x} (T(h(x,i),i) - S(x,i))^2 dx$$

$$+ \gamma \sum_{i=0}^{N_4-1} \int_{\Omega_x} (T(h(x,i),i) - T(x, N_4 - 1 - i))^2 dx$$

$$+ \chi \sum_{i=0}^{N_4-1} \int_{\Omega_x} \|h(x,i) - h^{-1}(x, N_4 - 1 - i)\|^2 dx$$

$$+ \rho \sum_{i=0}^{N_4-1} \int_{\Omega_x} \|Lu(x,i)\|^2 dx \tag{5}$$

where L is a symmetric differential operator that is used to help smooth and help prevent folding of the transformation. The choice of the operator L is based on the requirements

of the registration problem. In this paper, the Laplacian operator given by

$$Lu(x,t) = \alpha_1 \frac{\partial^2 u}{\partial x_1^2} + \alpha_2 \frac{\partial^2 u}{\partial x_2^2} + \alpha_3 \frac{\partial^2 u}{\partial x_3^2} + \alpha_4 \frac{\partial^2 u}{\partial t^2} \tag{6}$$

was used to regularize the transformation. For more realistic transformations, a linear-elastic differential operator L with the form

$$Lu(x,t) = -\alpha \nabla_{x,t}^2 u(x,t) - \beta \nabla_x (\nabla_x \cdot u(x,t)) + \gamma u(x,t) \tag{7}$$

could be used.

2.3. Transformation Parameterization

A 4D Fourier series representation is used to parameterize the displacement field u. Let $< \cdot, \cdot >$ represent the standard inner product. The continuous displacement field is defined to have the form

$$u_c(x,t) = \sum_k \eta_k e^{j<(x,t),\omega_k>} \tag{8}$$

for $x \in \Omega_x$ and $t \in \Omega_t$. The discrete transformation $h_d[n] = \frac{n}{N} + u[n]$ and its inverse $h_d^{-1}[n] = \frac{n}{N} + \tilde{u}[n]$ are defined in terms of the displacement fields

$$u_d[n] = \sum_k \mu_k e^{j<n,\omega_k>} \quad \text{and} \quad \tilde{u}_d[n] = \sum_k \tilde{\mu}_k e^{j<n,\omega_k>} \tag{9}$$

for $n \in \Omega_d$. The continuous and discrete displacement fields are related by the formula $u_d[n] = u_c(\frac{n_1}{N_1}, \frac{n_2}{N_2}, \frac{n_3}{N_3}, \frac{n_4}{N_4})$. The coefficients μ_k and $\tilde{\mu}_k$ are (3×1), complex-valued vectors with complex conjugate symmetry and $\omega_k = [\frac{2\pi k_1}{N_1}, \frac{2\pi k_2}{N_2}, \frac{2\pi k_3}{N_3}, \frac{2\pi k_4}{N_4}]$.

2.4. Estimation Procedure

The Fourier series parameterization in Eq. 9 is a multi-resolution decomposition of the displacement fields. Let

$\Omega_d[r] = \Omega_d \backslash \Omega'_d[r]$ represent a family of subsets of Ω_d where $\Omega'_d[r] = \{n \in \Omega_d | r_1 < n_1 < N_1 - r_1; r_2 < n_2 < N_2 - r_2; r_3 < n_3 < N_3 - r_3; r_4 < n_4 < N_4 - r_4\}$ and the set subtraction notation $A \backslash B$ is defined as all elements of A not in B. In practice, the low frequency basis coefficients are estimated before the higher ones allowing the global image features to be registered before the local features. This is accomplished by replacing Eq. 9 by

$$u_d[n, r] = \sum_{k \in \Omega_d[r]} \mu[k] e^{j<n, \theta[k]>}. \qquad (10)$$

where $r \in \Omega_d$ determines the number of harmonics used to represent the displacement fields. Define $h_d[n, r] = \frac{n}{N} + u_d[n, r]$ as a set of multi-resolution transformations. The components of r are initially set small and are periodically increased throughout the iterative minimization procedure. The set $\Omega_d[r]$ can be replaced by Ω_d when all of the components of r are greater than or equal to $(N-1)/2$ since the set $\Omega'_d[r]$ is empty. The constants r_1, r_2, r_3 and r_4 represent the largest x_1, x_2, x_3 and t harmonic components of the displacement fields. Each displacement field in Eq. 10 is efficiently computed using three $N_1 \times N_2 \times N_3 \times N_4$ FFTs, i.e., each component of the 3×1 vectors u_d is computed with a FFT after zeroing out the coefficients not present in the summations.

The image registration problem can be stated mathematically as the minimization of the cost function

$$C(\mu, r) = \sigma \sum_{n \in \Omega_d} |T_d[\bar{h}_d[n, r], n_4] - S_d[n]|^2$$

$$+ \gamma \sum_{n \in \Omega_d} |T_d[\bar{h}_d[n, r], n_4] - T_d[n_1, n_2, n_3, N_4 - n_4 - 1]|^2$$

$$+ \chi \sum_{n \in \Omega_d} ||u_d[n, r] - \tilde{u}_d[n_1, n_2, n_3, N_4 - n_4 - 1, r]||^2$$

$$+ \rho \sum_{n \in \Omega_d} ||L u_d(n, r)||^2 \quad (11)$$

with respect to $\{\hat{\mu}[k]\}$ where

$$\bar{h}_d[n, r] = \left[N_1 h_d^{(1)}[n, r], N_2 h_d^{(2)}[n, r], N_3 h_d^{(3)}[n, r] \right] \qquad (12)$$

is the normalized discrete transformation. The constants σ, γ, χ and ρ are used to enforce/balance the constraints.

The steps involved in estimating the basis coefficients μ are summarized in the following algorithm.

Algorithm

1. Set $\mu[k] = 0$ for $k \in \Omega_d$ and set $r = [1, 1, 1, 1]^T$.

2. Compute the displacement field $u_d[n, r]$ using Eq. 10.

3. Compute T from u, I_0, and I_1; set S equal to a time shifted version of T such that $S_d[n] = T_d[n_1, n_2, n_3, n_4 + 1]$.

4. Compute $h_d^{-1}[n, r]$ and set $\tilde{u}_d[n, r] = h_d^{-1}[n, r] - \frac{n}{N}$ for $0 \leq n_4 < N_4$.

5. Update the basis coefficients $\mu[k]$ using gradient descent.

6. If the criteria is met to increase the number of basis functions then set $r = r + 1$, and set the new coefficients in Eq. 10 to zero.

7. If the algorithm has not converged or reached the maximum number of iterations goto step 2.

8. Use the displacement field $u_d[n]$ to transform I_0 and I_1.

3. Results

The proposed algorithm was tested on the synthetic 2D images shown in Fig. 1. The first experiment was to deform the small square(I_0) into the big square(I_1) and vice versa. The dimension of the images were 64×64 pixels and the size of the squares were 12 by 12 and 32 by 32. Both squares were located at the center of the images. The time axis of the images was discretized into 8 equally spaced samples for this experiment. The parameter sets used for this experiment and the second experiment described below are shown in Table 1, where Δt was the gradient descent step size.

Δt	α	γ	σ	ρ	χ
0.00001	1.0	1.0	1.0	0.0001	1000.0

Table 1. Parameter set for experiments.

The results of transforming the small square into the large square and back again are presented in Figure 3. Each row of Figure 3 corresponds to a time index starting at time $n_4 = 0$ for the top row and progressing to time $n_4 = 7$ for the bottom row. The first column shows how the template image T was initialized for the gradient descent procedure; the first four time samples $T(x, 0) - T(x, 3)$ were set equal to image I_0 and the second four times samples $T(x, 4) - T(x, 7)$ were set equal to image I_1. The second column shows the intermediate deformed images $T(h(x, 0), 0) - T(h(x, 7), 7)$ after 2000 iterations of gradient descent. The top four images in the third column show the absolute difference between the images $T(h(x, 0), 0) - T(h(x, 3), 3)$ and image I_1 and the bottom four images show the absolute difference between the images $T(h(x, 4), 4) - T(h(x, 7), 7)$

and image I_0. The nearly black difference image in the fourth and eighth images of column three show that the small square was transformed into the shape of the large square and the large square was transformed into the shape of the small square, respectively. The images in columns 2 and 3 also demonstrate the periodic nature of the template T in time and show that the shape of the intermediate images are equally spaced in time. The images of the fourth and fifth columns show the accumulated displacement fields[3] in the x and y dimensions, respectively, where black denotes a negative displacement and white denotes a positive displacement. Columns six and seven show the Jacobian of the accumulated transformations and the result of applying the accumulated transformations to a rectangular grid. The values of the Jacobian[4] ranged from 0.51 to 2.0 for the intermediate transformations and from 0.10 to 2.4 for the concatenated transformations from the small square to the large square and from 0.38 to 9.7 for the transformation of the large square to the small square. The maximum inverse consistency error for this experiment was 0.64 pixels. The results were computed on a 500MHz, 21264 alpha processor and took about 560 seconds for the 2000 iterations.

In the second experiment, the image containing the "C" shown in Fig. 1 was deformed into the shape of the circle and vice versa. Unlike the first experiment, the transformation of the "C" to the circle requires a nonlinear transformation. The dimensions of the images were 64×64 pixels. The height and width of the outer contour of the "C" object was 18 and 16 pixels, respectively. The distance from the outer to inner contour was 8 pixels and the two ends were separated by 13 background pixels. The radius of the circle object was 14 pixels. The results of running the algorithm for 3000 iterations of gradient descent are shown in Figure 4. The description of the panels in this figure are equivalent to those in Fig. 3 except that the time axis was discretized into 12 time samples instead of 8. Twelve time samples were required for this deformation due to the locally large nonlinear deformations required for this registration. The Jacobian and grid images show that the "C" was deformed into shape of the circle by expanding the "C" along the interior contour to fill the void. The outside contour of the "C" remained relatively fixed in space during the deformation. Likewise, the circle was transformed into the shape of the "C" by indenting the circle at the opening of the "C". This indentation increased until it formed the inner contour of the "C". The values of the Jacobian ranged from 0.38 to 2.5 for the intermediate transformations and from 0.42

---

[3]The ith row corresponds to the accumulation of time points $t = 0$ to $t = i$ for the first four rows and of times $t = 4$ to $t = i$ for the last four rows.

[4]The Jacobian values were calculated with respect to a Eulerian coordinate system. In a Eulerian coordinate system, an expansion corresponds to a Jacobian value less than 1 and a shrinking corresponds to a Jacobian value greater than 1.
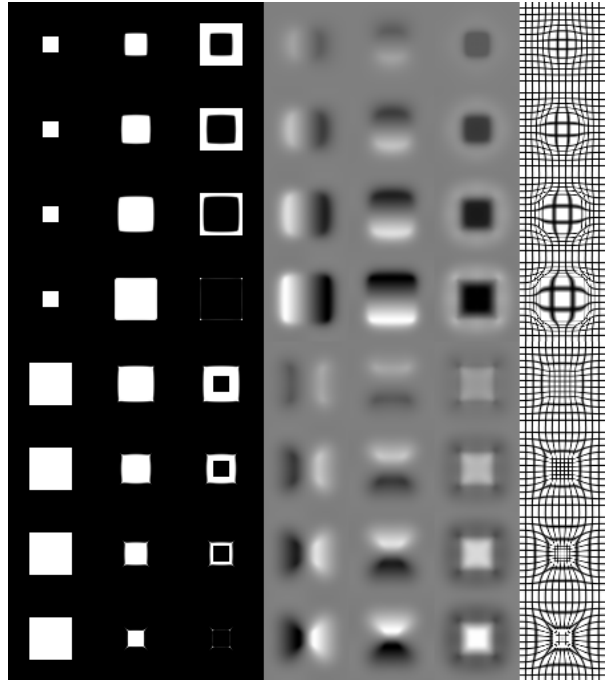
Figure 3. Registration between small and big squares. Each row corresponds to a point on the time axis. Column 1 shows the initialization of the template before gradient descent. Column 2 shows the incrementally deformed template images after gradient descent. Column 3 shows absolute difference images between the incrementally deformed template images and their corresponding target images. Column 4 and 5 shows the accumulated x- and y-displacement fields, respectively. Column 6 shows the accumulated Jacobian images. Column 7 shows the accumulated deformed grid image.

to 8.1 for the concatenated transformations from the "C" to the circle and from 0.10 to 2.1 for the transformation of the circle to the "C". The maximum inverse consistency error for this experiment was 3.0 pixels.

4. Discussion

4.1. Temporal Sampling Rate

The number of intermediate template images or transformations between the original images is referred to as the temporal sampling rate. The number of temporal samples required to match two images is a function of the degree of deformation between the two images. A large number

of samples is required if there is a large deformation between the pair of images being registered. A small number or no samples are required in the case of a small deformation between image pairs. Minimizing the number of temporal samples has the advantage of reducing computer computation and storage requirements.

The number of temporal samples can be determined empirically by picking an initial sampling rate and registering the images. The number of samples should be reduced if there is relatively little deformation as measured by the Jacobian of the intermediate transformations. As a rule of thumb, the number of temporal samples may be reduced until the minimum of $\text{Jacobian}(h(x, i))$ and $1/\text{Jacobian}(h(x, i))$ for $x \in \Omega_x$ and $0 \leq i < N_4$ of the final transformation is greater than 0.5. Likewise, the number of temporal samples should be increased until the minimum of $\text{Jacobian}(h(x, i))$ and $1/\text{Jacobian}(h(x, i))$ is greater than 0.5.

5. Summary and Conclusions

We presented a new elastic image registration approach that accommodates large, non-linear deformations while constraining the forward and reverse transformations to be inverses of one another. The feasibility of the algorithm for accommodating nonlinear deformations was demonstrated in 2D by deforming an image containing a C-shaped object into the shape of a circle and vice versa. In future work, we plan to study the sensitivity of the algorithm to the parameters and generate registrations of 3D images.

6. Acknowledgments

References

[1] M. Bro-Nielsen and C. Gramkow. Fast fluid registration of medical images. In K. H. Höhne and R. Kikinis, editors, *Visualization in Biomedical Computing*, volume 1131, pages 267–276. Springer, Hamburg, Germany, 1996.

[2] G. Christensen. Consistent linear-elastic transformations for image matching. In A. Kuba and M. Samal, editors, *Information Processing in Medical Imaging*, LCNS 1613, pages 224–237. Springer-Verlag, June 1999.

[3] G. Christensen. *Deformable Shape Models for Anatomy*. D.Sc. Dissertation, Department of Electrical Engineering, Sever Institute of Technology, Washington University, St. Louis, MO. 63130, Aug 1994.

[4] G. Christensen and H. Johnson. Consistent image registration. *IEEE Transactions on Medical Imaging*, 20(7):568–582, July 2001.

[5] G. Christensen, R. Rabbitt, and M. Miller. Deformable templates using large deformation kinematics. *IEEE Transactions on Image Processing*, 5(10):1435–1447, Oct 1996.

[6] H. Johnson and G. Christensen. Landmark and intensity-based, consistent thin-plate spline image registration. In M. Issana and R. Leahy, editors, *Information Processing in Medical Imaging*, LCNS 2082, pages 329–343. Springer-Verlag, June 2001.

[7] S. Joshi. *Large deformation diffeomorphisms and Gaussian random fields for statistical characterization of brain submanifolds*. D.Sc. Dissertation, Department of Electrical Engineering, Sever Institute of Technology, Washington University, St. Louis, MO. 63130, Dec 1997.

[8] S. Joshi and M. I. Miller. Landmark matching via large deformation diffeomorphisms. *IEEE Transactions on Image Processing*, 9(8):1357–1370, August 2000.

[9] H. Lester, S. Arridge, K. Jansons, L. Lemieux, J. Hajnal, and A. Oatridge. Non-linear registration with the variable viscosity fluid algorithm. In A. Kuba and M. Samal, editors, *Information Processing in Medical Imaging*, LCNS 1613, pages 238–251. Springer-Verlag, June 1999.

[10] R. Rabbitt, J. Wiess, G. Christensen, and M. Miller. Mapping of hyperelastic deformable templates using the finite element method. In R. Melter, A. Wu, F. Bookstein, and W. Green, editors, *Vision Geometry IV*, Proceedings of SPIE Vol. 2573, pages 252–265, 1995.

[11] J. Thirion. Image matching as a diffusion process: an analogy with maxwell's demons. *Medical Image Analysis*, 2:243–260, 1998.

[12] R. Woods, S. Grafton, J. Watson, N. Sicotte, and J. Mazziotta. Automated Image Registration: II. Intersubject Validation of Linear and Nonlinear Models. *Journal of Computer Assisted Tomography*, 22(1):153–165, 1998.
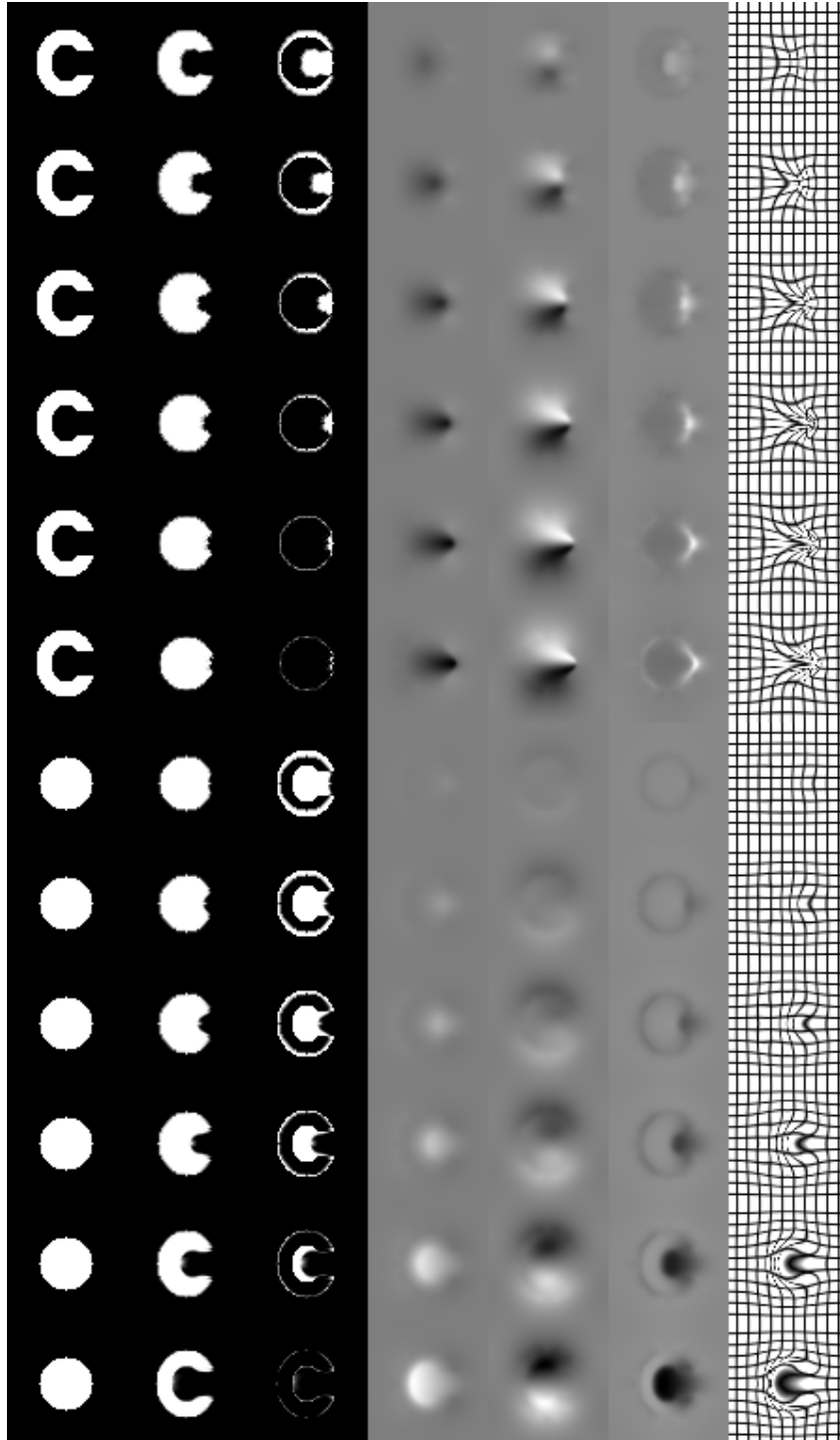
Figure 4. Registration between a C and a circle. Each row corresponds to a point on the time axis. Column 1 shows the initialization of the template before gradient descent. Column 2 shows the incrementally deformed template images after gradient descent. Column 3 shows absolute difference images between the incrementally deformed template images and their corresponding target images. Column 4 and 5 shows the accumulated x- and y-displacement fields, respectively. Column 6 shows the accumulated Jacobian images. Column 7 shows the accumulated deformed grid image.